CHAPTER 3

EXPERIMENTAL PROCEDURE AND SAMPLE CHARACTERIZATIONS

This chapter gives a brief description of the experimental setup including experimental procedure which used for prepare colloidal TiO_2 and Fe_2O_3 NPs. Moreover, the sample characterizations such as morphological, structural and optical properties are described. Photocatalytic and antibacterial activities of the samples are examined.

3.1 Synthesis of TiO_2 NPs by sparking process

3.1.1 Experimental setup and experimental procedure

In this part, the sparking of two sharp titanium tips for preparation of TiO_2 NPs were done in a glass bottle filled with 10 mL distilled water. The two sharp titanium tips (∅ 0.25 mm, purity 99.8 %, typical impurity analysis are composed of N, C, H, Fe and O in amount of 30, 30, 11, 250 and 540 ppm, respectively., Advent Research Material, Ltd.) were prepared by cutting with pliers and placed horizontally at 3 mm spacing (d) and 2 mm above a water level (h). The schematic diagram of the sparking was shown in Figure 3.1.

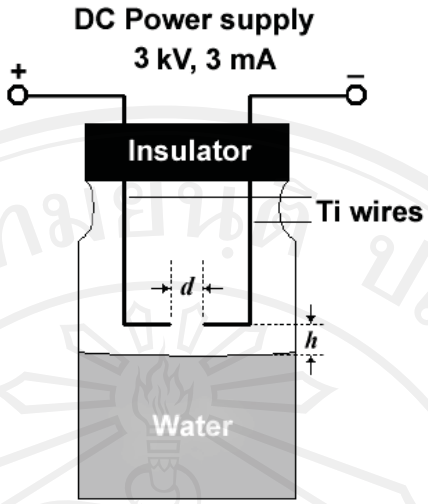

Figure 3.1 Schematic diagrams of the sparking apparatus

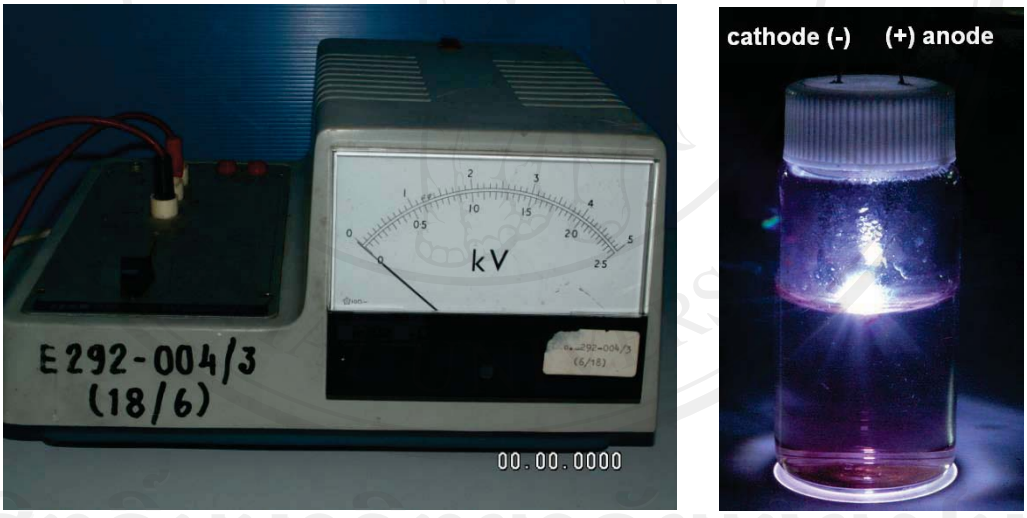

(a) (b)

Figure 3.2 (a) High DC voltage power supply and (b) an experiment

As schematically depicted in Figure 3.1, the high DC voltage power supply (Figure 3.2a) for a sparking voltage of ~3 kV with a limited current of 3 mA was connected to the apparatus. The NPs were then continuously deposited into the water

(see Figure 3.2b) by the sparking for 1 to 5 h. The NP-dispersed water was obtained and separated for further characterizations.

3.1.2 Sample characterization

TiO_2 NPs were deposited on quartz substrates (1×10×10 mm^3) by two drops of the NP-dispersed water. The deposited samples were annealed at 250 and 500 °C in air for 1 h. The morphologies were observed by SEM (JEOL JSM-6335F). The particle sizes and structural properties of the NPs were investigated by TEM (JEOL JEM-2010) and Raman spectrometer (JOBIN YVON HORIBA T64000) with a 514.5 nm argon ion laser at room temperature. The optical properties were measured in the visible region by UV-vis spectrophotometer (Perkin Elmer Instruments). The transmittance spectra were analyzed using the modified envelope method, which allows the absorption coefficient to be determined.

The photocatalytic properties of the obtained colloidal TiO_2 NPs at 1.0 vol % of 0.01 mM methylene blue (MB) solution (Ajax Finechem) were investigated by measuring the photocatalytic decomposition under sunbath for 1 h. Variation in the concentration of MB was monitored by UV–vis spectroscopy.

Anti-bacterial activity which was examined by TiO_2 NPs can be done by using *E.coli* TISTR 527 which was selected as the common indicator bacteria [62,63]. Luria agar (LA; Miller, Cat. No. C6011) was prepared by an addition of 10 g casein peptone, 10 g sodium chloride and 5 g yeast into 1 L of deionized water followed by an addition 15 g of agar. The medium was autoclaved at 121 °C for 15 min. *E.coli* standard was then inoculated on LA and incubated at 37 °C for 24 h. Cell cultures

were diluted to approximately 10^8 colony forming unit per milliliter (CFU/mL) in order to comparison with standard 0.5 Mc Farland.

The process of bactericidal activity testing on Gram-negative bacteria was prepared as shown in Figure 3.3.

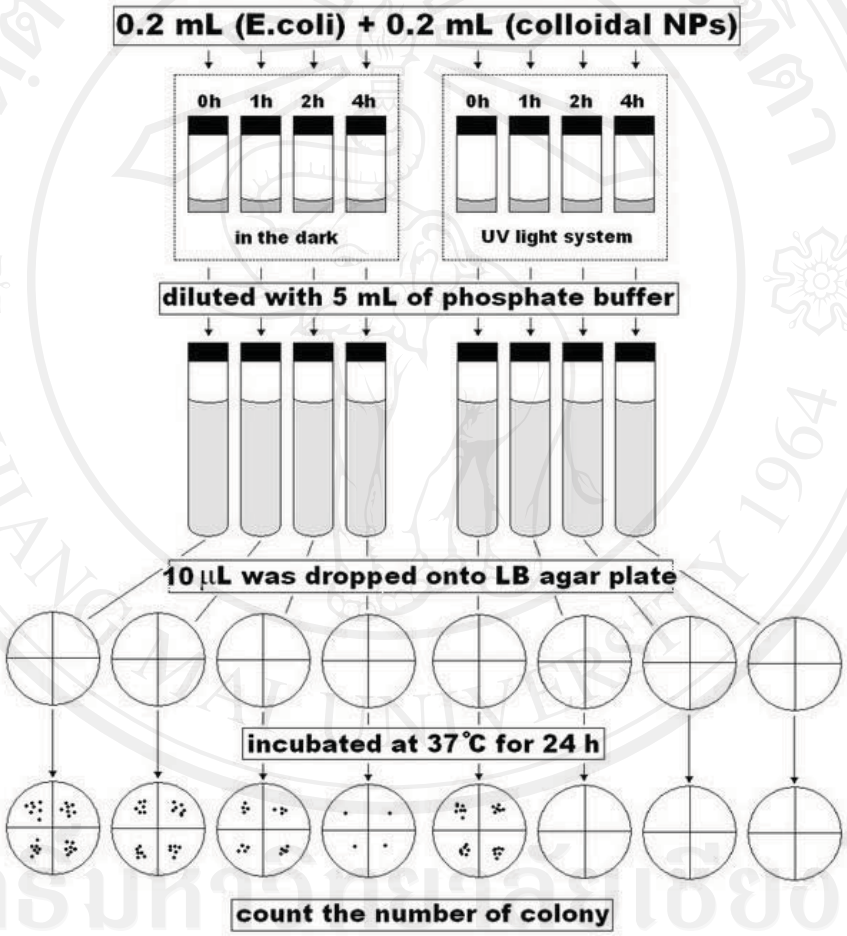

Figure 3.3 Flow chart of the experimental procedures to study antibacterial activity of TiO_2 NPs.

Diluted *E.coli* 0.2 mL were treated with 0.2 mL of colloidal TiO_2 NPs (1-5 nm in diameter in a concentration of 0.25 mg/mL) [64]. The samples were then kept in

the dark and under UV light (UVA; Philip 6W) for 0, 1, 2 and 4 h. Each condition was diluted by 5 mL of phosphate buffer, dropped off 10 µL onto agar plate and incubated at 37 °C. The colony counts were taken at 24 h after incubation. The morphology and microstructure of bacteria cells were observed by scanning electron microscopy (SEM, JEOL JSM-6335F) and transmission electron microscopy (TEM, JEOL JEM-2010) which the sections were cut at a thickness of 80 nm by a microtome.

Standard preparation for TEM analysis

Process diagram of standard preparation for TEM analysis was shown in Figure 3.4

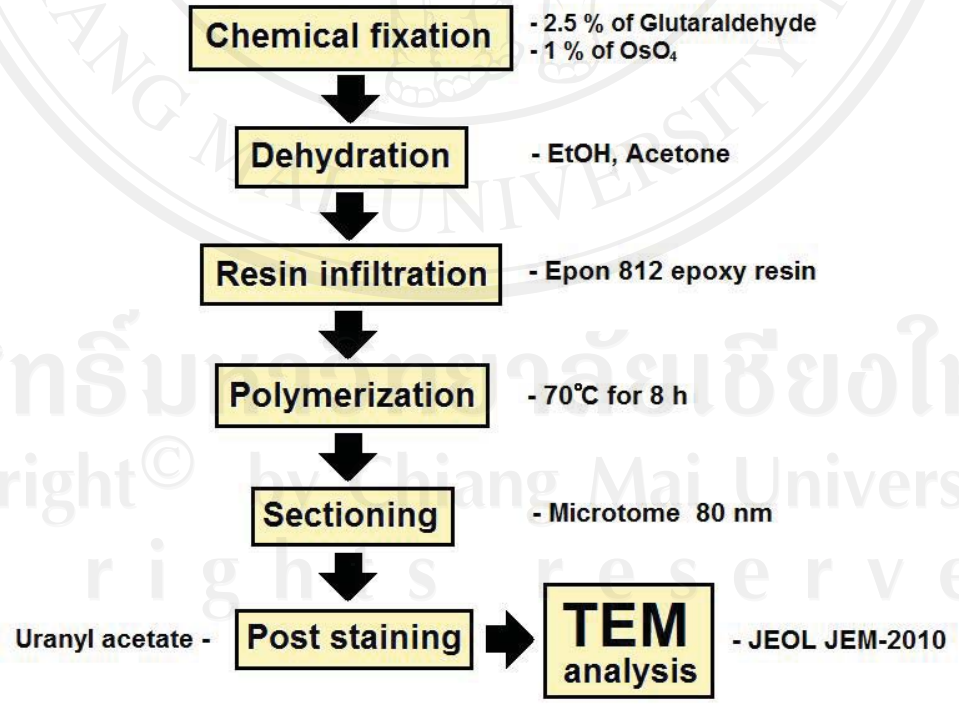

Figure 3.4 standard preparations for TEM analysis

Firstly, fixation process is the first and most important step in any TEM study. The reason is cross-link cellular structures into a matrix so as to preserve the structure of the cells with the minimum of alteration from the living state. Moreover, this process can be protect and stabilize cellular structures from changes during subsequent treatments and from irradiation by the electron beam.

Second is dehydration process. This was generally performed by using ethanol (E*t*OH) and acetone to replace water in incompatible with conditions inside an electron column. Most of the materials used to infiltrate and embed specimens prior to ultrathin sectioning are hydrophobic.

Third is resin infiltration process, normally Epon 812 epoxy resin is used to embed the specimens. This is potentially more dangerous than the fixatives. Many of the resin components are known to cause cancer in rats or mice. During the embedding process the resins are dissolved in solvent(s) that can carry the resin into your skin even through plastic gloves. In contrast to fixatives, whose actions are immediate and apparent, the consequences of exposure to the resins are not apparent for years. Therefore careful handling of all resins prior to polymerization into hard blocks should be taken.

Fourth is polymerization process which is generally done at 70 °C for 8 h for the glutaraldehyde and osmium fixatives. As alternatives cacodylate, PIPES or HEPES buffer can be used instead. The type of buffer in which the fixatives are made up can affect the appearance of the specimen. However, one advantage of cacodylate and PIPES or HEPES is that $CaCl_2$ and/or $MgCl_2$ can be added to the primary fixative. Calcium (and Mg) ions reduce the extraction of cellular components and also enhance the retention of phospholipids.

Fifth is sectioning process, normally used “Microtome” which is a sectioning instrument that allows the cutting of extremely thin slices of material, known as sections. Microtomes are an important device in microscopy preparation, allowing for the preparation of samples for observation under transmitted light or electron radiation. Steel, glass, or diamond blades can be used in microtome depending upon the specimen being sliced and the desired thickness of the sections being cut. Steel blades are used to prepare sections of animal or plant tissues for light microscopy histology. Glass knives are used to slice sections for light microscopy and to slice very thin sections for electron microscopy. Industrial grade diamond knives are used to slice hard materials such as bone, teeth and plant matter for both light microscopy and for electron microscopy. Gem quality diamond knives are used for slicing thin sections for electron microscopy.

Sixth, Post staining is a biological tissue which has little inherent contrast in either the light or electron microscope. Staining is employed to give both contrasts to the tissue as well as highlighting particular features of interest.

3.2 Synthesis of Fe_2O_3 NPs by pyrosol method

3.2.1 Experimental setup and experimental procedure

Fe_2O_3 NPs were prepared inside a tube furnace as shown in Figure 3.5.

Figure 3.5 The experimental setup

The experiment was carried out using a tube furnace (a), an internal diameter of 19 mm and length of 750 mm. The tube was connected to a three way tube (b) containing an aqueous iron (III) nitrate ($Fe(NO_3)_3.9H_2O$) solution (c) at concentrations of 1, 0.1 and 0.01 M. A mist generator (1.7 MHz) (f) was immerged in water (e) and placed under the solution, which was separated from water using a plastic film (d). The process starts from aerosol generation of precursor solution which containing Fe^+ ions was then atomized by the mist generator. The aerosol was subsequently brought into the tube furnace (g) by a controlled flowing air stream (340 ml/min) at 350 ºC.

3.2.2 Sample characterization

The particle sizes were characterized by scanning electron microscope (SEM :JEOL, JSM-6335F). Structural properties were examined by XRD (Bruker D8Advance) using Cu-Kα radiation operated at 40 kV and 30 mA in the scanning angle (2θ) from 20° to 80°. The step scan and step time was kept at 0.02° and 1 sec, respectively and Raman spectrum were taken using Raman spectrometer(JOBIN YVON HORIBA; T64000) which have a 514 nm line of Ar ion laser with a power of 50 mW as the light source in the backscattering geometry at room temperature.

3.3 Measurement instruments

This section provides an overview of the sample characterization which was used to obtain the information on the properties of TiO_2 NPs. This includes scanning electron microscopy (SEM) which was used for determination of the morphology, surface properties of the obtained NPs and also thickness measurement of NP thin films. Moreover, the morphology with a high resolution including their structural properties can be characterized by transmission electron microscopy (TEM). Structural properties of the NPs and NP thin films samples were characterized by Diffraction pattern (TEM), Raman spectroscopy. Moreover, wettability of the films was measured by contact angle measurement.

The NPs were characterized by the following techniques:

3.3.1 Scanning electron microscopy (SEM)

In this study, the samples were analyzed using JEOL JSM-6335F environmental field-emission (FE) SEM as shown in Figure 3.6. It was used to

determine the morphology of the NPs and NP thin films. The samples were pasted on the brass sample holder without gold coating. Therefore, an electric potential was used with low accelerating voltage (1-3 kV).

Figure 3.6 Scanning electron microscope

3.3.2 Transmission Electron Microscopy (TEM)

A Transmission electron microscopy (TEM) was employed to investigate the morphology, particle size distribution, elemental composition and crystallography of the NPs. Samples for TEM were prepared by dropping colloidal NPs on the copper grids with a carbon film, left it dry in the air. The samples were investigated by TEM (JEOL JEM 2010 microscope) operated at 200 kV accelerating voltage (Figure 3.7).

Figure 3.7 Transmission electron microscope

3.3.3 X-ray diffraction (XRD)

X-ray crystallography is a method of determining the arrangement of atoms within a crystal, in which a beam of X-rays strikes a crystal and scatters into many different directions. X-ray diffraction is based on constructive interference of monochromatic X-rays and a crystalline sample. These X-rays are generated by a cathode ray tube, filtered to produce monochromatic radiation, collimated to concentrate, and directed toward the sample. The interaction of the incident rays with the sample produces interference when conditions satisfy Bragg's Law:

$$2d\sin\theta = n\lambda \qquad (3.1)$$

where d is the spacing between diffracting planes, θ is the incident angle, n is any integer, and λ is the wavelength of the beam.

This law relates the wavelength of electromagnetic radiation to the diffraction angle and the lattice spacing in a crystalline sample. These diffracted X-rays are then detected, processed and counted. By scanning the sample through a range of 2θ angles, all possible diffraction directions of the lattice should be attained due to the random orientation of the material. Conversion of the diffraction peaks to d-spacings allows identification of the compound because each compound has a set of unique d-spacings. Typically, this is achieved by comparison of d-spacings with standard reference patterns.

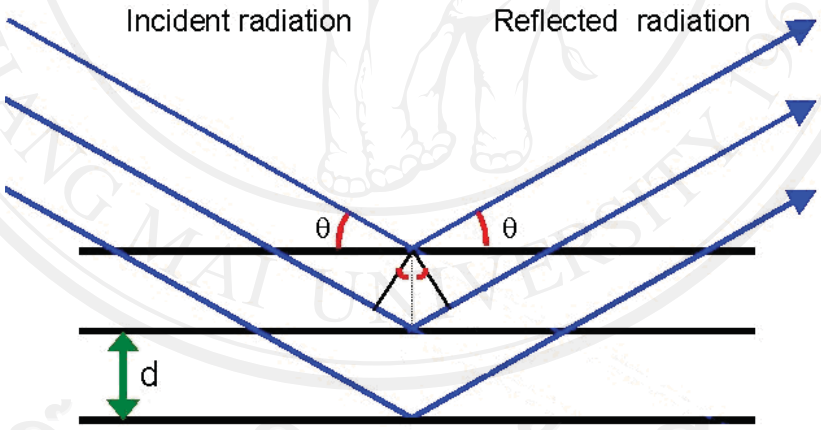

Figure 3.8 X-Ray diffraction. [65]

3.3.4 Raman spectroscopy

Micro-Raman spectroscopy was used for characterization of structural properties of the samples. In this work, we was performed using a Horiba; Jobin Yuon-T 64000 with an Ar ion laser (514.5 nm) at 500X magnification (~2 μm spot size), as shown in Figure 3.9.

Figure 3.9 Raman spectroscope

Raman spectroscopy is the measurement of the wavelength and intensity of inelastically scattering of monochromatic light, usually from a laser in the visible, near infrared and near ultraviolet range, from molecules. Laser can be used as the excitation source. In conventional Raman spectroscopy, visible lasers are used (e.g., Ar^+, Kr^+, Nd:YAG, He-Ne, diode) to stimulate the molecules to high energy “Virtual”

states of excitation. A Raman photon is emitted if a molecule undergoes a transition to a higher vibrational energy state than its original state (Stokes Raman scattering), a lower energy vibrational state (Anti-Stokes Raman scattering) and the original state (Rayleigh scattering) which shown in Figure 3.10. Normally, Stokes Raman scattering has higher intensity.

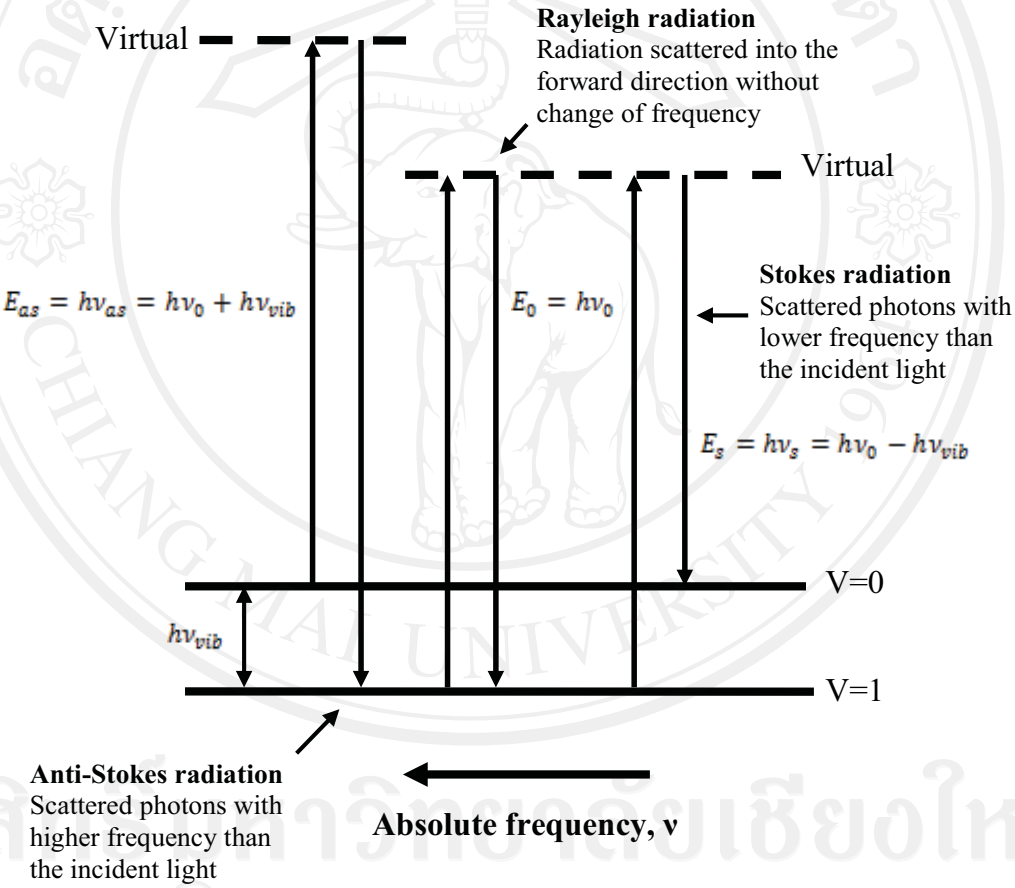

Figure 3.10 Raman scattering [66]

3.3.5 UV-vis spectroscopy

Optical transmittances and absorbance were carried out in the range of 300 to 800 nm using UV-vis spectrophotometer (Hitachi U-4100) as shown in Figure 3.11.

Figure 3.11 UV-vis spectroscope

From the absorption equation of light by the medium is quantified by

$$I = I_0 e^{-\alpha t} \qquad (3.2)$$

From the literature, there are three values of absorption coefficient.

$$\alpha_1 = \frac{1}{t}\ln\frac{(1-R)}{T} \qquad (3.3)\ [67]$$

$$\alpha_2 = -\ln T \qquad (3.4)\ [68]$$

$$\alpha_3 = \frac{(1-C)^2}{2C} \qquad (3.5)\ [69]$$

where t is film thickness, R is reflectance and T is transmittance. Consider $I_0 = 1$ and I = Transmittance, so equation 3.2 can be written as

$$T = e^{-\alpha t}$$

$$\ln T = \ln e^{-\alpha t}$$

$$-\alpha t = \ln T$$

$$\alpha = (1/t)(-\ln T)$$

$$\alpha_1 = (1/t)(\ln 1/T) \qquad (3.6)$$

but there is the reflectance of light so equation 2.5 becomes

$$\alpha_1 = (1/t)(\ln (1-R)/T) \qquad (3.7)$$

Consider equation 3.7, thickness of the film has no any influence on absorbance coefficient and reflectance is very less compared to transmittance and absorbance so, equation 3.7 can be written as

$$\alpha_2 = \ln 1/T = -\ln T \qquad (3.8)$$

Moreover, the absorption coefficient can be derived from the simple treatment related to the absorption transitions between direct parabolic bands (see Figure 3.12). The absorption coefficient can be expressed as

$$\alpha(h\nu) = A\sum P_{if} n_i n_f \qquad (3.9)$$

where P_{if} is the transition probability, n_i and n_f are the intensities of electrons in the initial state and of empty energy levels in the final state, respectively, and the sum is over all initial and final state.

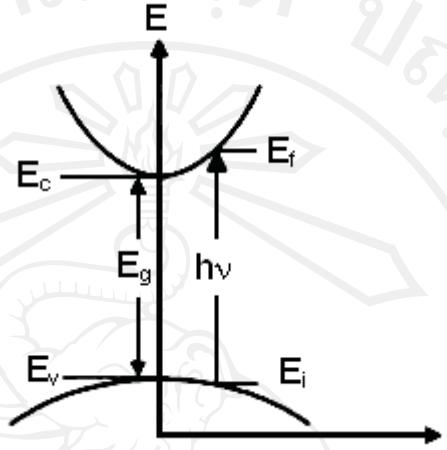

Figure 3.12 Schematic diagram of the absorption transitions between direct parabolic bands. [70]

The energy associated with a given state is given by

$$E = \frac{\hbar^2 k^2}{2m} \tag{3.10}$$

Thus, the electron energy (relative to E_c), $E_c = (\hbar^2 k^2)/2m_e^*$ and the hole energy (relative to E_v), $E_h = (\hbar^2 k^2)/2m_h^*$. Using this equation, the transition energy can be expressed as

$$h\nu = \frac{h^2 k^2}{2m_e^*} + \frac{h^2 k^2}{2m_h^*} + E_g \tag{3.11}$$

and

$$h\nu - E_g = \frac{h^2k^2}{2m_e^*} + \frac{h^2k^2}{2m_h^*} = \frac{\hbar^2k^2}{2m_r^*} \qquad (3.12)$$

where $m_r^* = m_e^* m_h^* / (m_e^* + m_h^*)$ is the reduced effective mass. The general expression for the density of state in $N(E)dE = (2\pi^2\hbar^3)^{-1}(2m^*)^{3/2}E^{1/2}dE$, and thus, for this case, the density of state can be written as

$$N(h\nu)d(h\nu) = (2\pi^2\hbar^3)^{-1}(2m_r^*)^{3/2}(h\nu - E_g)^{1/2}d(h\nu) \qquad (3.13)$$

Thus, for direct transitions between parabolic valence and conduction bands the absorption coefficient is

$$(\alpha h\nu)^2 = A(h\nu - E_g) \qquad (3.14)$$

where A is a constant, the energy gap E_g and $h\nu$ are in eV.

Energy gap of the films was estimated from the optical measurements, using equation 3.14. To determine energy gap, the variation of $(\alpha h\nu)^2$ versus $h\nu$ were plotted. Extrapolation of linear portion to the energy axis gives the band gap energy.